Higher-order field effects in pion absorption on two nucleons

G. Kälbermann and J. M. Eisenberg
Department of Physics and Astronomy, Tel Aviv University, 69978 Tel Aviv, Israel
(Received 30 November 1982)

We estimate the importance of rescattering diagrams involving intrinsically third-order effects in the pionic field for the process of pion absorption at rest on a pair of nucleons. The calculation is performed using a chiral bag model adapted for the correct description of higher-order pionic effects. The model provides the form factors needed in order to achieve a convergent result. The third-order diagrams cancel in part; nevertheless, the net result is as important as the conventional second-order s-wave rescattering mechanism for reasonable bag radii $R \sim 1$ fm and becomes dominant for bag radii $R \lesssim 0.7$ fm for internucleon distances less than about 2 fm.

[NUCLEAR REACTIONS $(\pi,2N)$, pion absorption, chiral bag models.]

I. INTRODUCTION

The process of pion absorption on a pair of nucleons is often described in terms of direct absorption (Fig. 1) and s- or p-wave rescattering diagrams (Fig. 2). It was shown some time ago[1] that rescattering terms are quite important for the calculation of the absorption rate. More recently,[2] it was demonstrated that the nn/np emission ratio in nuclei after π^- absorption is very sensitive to the inclusion of rescattering terms in the absorption operator.

The question of the possible importance of higher-order rescattering diagrams must be treated within the framework of some field theory model. These terms often appear naturally as higher-order elements in a Lagrangian whose lowest orders give rise to the interactions of the direct absorption and s- or p-wave rescattering. Weinberg's[3] chiral Lagrangian is widely accepted as a good basis for this purpose. If one attempts to calculate the diagrams of higher-order rescattering using this Lagrangian one encounters the diagrams depicted in Fig. 3, and a divergent result is obtained for point interactions, so that the need for cutoff factors is immediately apparent. These form factors are unfortunately not well known, and especially the $\pi\pi\pi NN$ vertex requires a model for its treatment, so that the calculation of these diagrams inevitably requires specific assumptions concerning the internal behavior of the hadrons.

In recent years chiral bag models have become a helpful tool for the investigation of pion-nucleon interactions.[4–6] In particular, one version[7,8] of the bag model allows for the description of pion-nucleon processes up to third order in the πNN coupling constant g. To first and second order the effective Lagrangian of this approach is identical to the cloudy bag model (CBM),[5,6] while for reactions that depend on the third-order interaction g^3, such as $\pi N \to \pi\pi N$, it yields more immediate agreement with experiment. This form of the chiral bag model is especially well suited to clarify the extent to which the higher-order effects of Fig. 3 enter in the $(\pi,2N)$ process.

Chiral bag models are most straightforwardly ap-

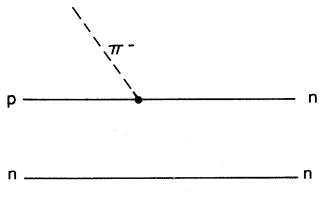

FIG. 1. Direct absorption diagram (previous or subsequent NN interactions have been suppressed).

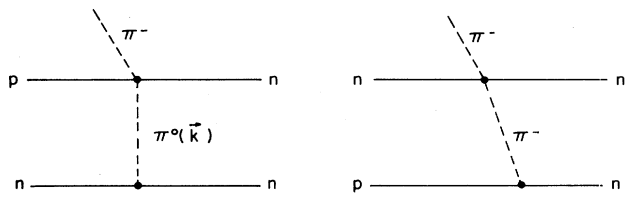

FIG. 2. Single-pion exchange rescattering diagrams.

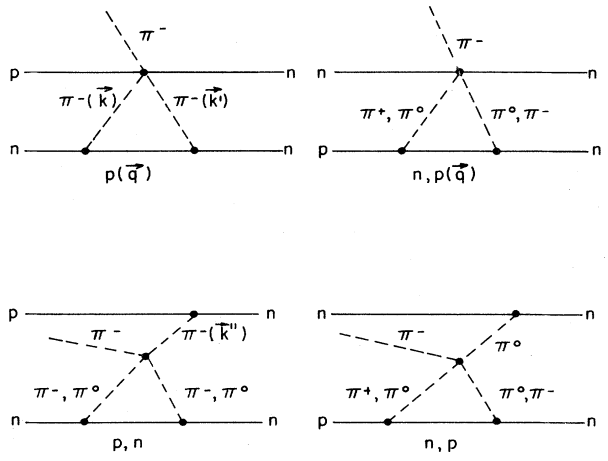

FIG. 3. Rescattering diagrams (of order g^5).

plied at moderate nucleon energies (say less than about 100 MeV) at which the nucleon can be approximately considered to be at rest, so that one may use the static cavity solutions of the MIT bag model.[9,10] At the present time no translationally invariant chiral bag model is available, especially because of the lack of physical understanding of the bag surface in terms of field operators. Nevertheless, the bag model determines the πN form factor as a function of the bag radius R, and thus gives a direct answer for the calculation of the diagrams of Fig. 3 if recoil effects are neglected or treated approximately. In this spirit we use our version[7] of the chiral bag model to calculate the third-order diagrams. As a benchmark for comparison we consider them in relationship to the well-known and often-used second-order rescattering graphs[1,2] of Fig. 2. We note that there exist other categories of diagrams of the same order as those of Fig. 3, which for one reason or another are not considered here. For example, the cases shown in Fig. 4(a) vanish identically for pion absorption at rest. This is because the p-wave vertices (with one or three pion lines) and momentum conservation introduce a symmetric factor $\vec{k}+\vec{k}'$ in each graph, while the s-wave, two-pion vertex involves the antisymmetric combination $\omega(k)-\omega(k')$ for pion energy ω, so that after integration over the internal variables $\vec{k},\vec{k}'$ the contribution is zero. The graphs of Fig. 4(b) are omitted because they represent part of the conventional rescattering process which is a straightforward extension of the usual methods of calculation.[1,2] Naturally there are still other effects which may enter into the $NN\pi\to NN$ interaction, as for example, Δ admixtures, but our purpose is merely to establish the significance of the third-order effects for use in constructing the two-nucleon transition operator on $(\pi,2N)$, and so we have not considered these complications here.

II. THE RESCATTERING DIAGRAMS

The chiral bag model that we use is defined by the following Lagrangian:

$$\mathcal{L}=\sum_a\left[\frac{i}{2}\bar{q}_a\overleftrightarrow{\partial}q_a-B\right]\theta_v-\tfrac{1}{2}\sum_a\bar{q}_aq_a\Delta_s+\sum_a\bar{q}_a\gamma^\mu\frac{1}{(1+g^2\vec{\pi}^2)}[g\gamma_5\vec{\tau}\cdot\partial_\mu\vec{\pi}-g^2\vec{\tau}\cdot(\vec{\pi}\times\partial_\mu\vec{\pi})]q_a\theta_v$$
$$+\frac{1}{2}\frac{1}{(1+g^2\vec{\pi}^2)^2}\partial^\mu\vec{\pi}\cdot\partial_\mu\vec{\pi}-\frac{1}{2}\frac{1}{(1+g^2\vec{\pi}^2)}m^2\vec{\pi}^2\,, \tag{1}$$

where q_a is the quark field of flavor a, $\vec{\pi}$ is the pionic field, $\theta_v=\Theta(R-r)$ is the step function for the bag of radius R, Δ_s is the bag surface delta function, and g is the πN coupling constant. The terms entering the calculation of the diagrams of Figs. 2 and 3 are the following:

$$\mathcal{L}_{\pi qq}=g\sum_a\bar{q}_a\gamma^\mu\gamma_5\vec{\tau}\cdot\partial_\mu\vec{\pi}q_a\theta_v\,, \tag{2}$$

$$\mathcal{L}_{\pi\pi qq}=-g^2\sum_a\bar{q}_a\gamma^\mu\vec{\tau}\cdot(\vec{\pi}\times\partial_\mu\vec{\pi})q_a\theta_v\,, \tag{3}$$

$$\mathcal{L}_{\pi\pi\pi qq}=-g^3\sum_a\bar{q}_a\gamma^\mu\gamma_5\vec{\tau}\cdot\partial_\mu\vec{\pi}\vec{\pi}^2q_a\theta_v\,, \tag{4}$$

$$\mathcal{L}_{\pi\pi\pi\pi}=\tfrac{1}{2}m^2g^2\vec{\pi}^4-g^2\partial_\mu\vec{\pi}\cdot\partial^\mu\vec{\pi}\vec{\pi}^2\,. \tag{5}$$

The time components ($\mu=0$) of Eqs. (2) and (4) vanish when the static cavity solutions[9,10] are used. (In the case of Weinberg's Lagrangian these terms vanish in the nonrelativistic reduction.) Equations (2)—(5) have equivalent expressions in Weinberg's Lagrangian when the nucleon field is used instead of the quark field; the construction here of the nucleon out of quarks produces the appropriate form factors for the vertices of Eqs. (2)—(4). When these vertices are used in the calculation of the diagrams in Fig. 3, the expressions involve linearly either the momen-

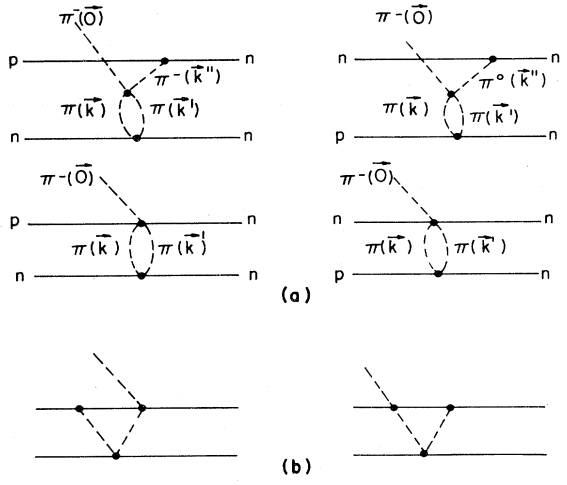

FIG. 4. (a) Two diagrams of fifth order that vanish here. (b) A fifth-order diagram that we classify as a rescattering effect.

tum of the external absorbed pion or the momenta of the rescattered pions. For the (s-wave) absorption of low momentum pions, only the latter case survives.

In Eq. (2) the most important contribution comes from the time component ($\mu=0$). In order to perform the calculation, and in the spirit of the recoilless approximation, we fix each of the two nucleons at its respective position, $\vec{r}_1$ and $\vec{r}_2$, throughout the dynamic process, and subsequently vary the internucleon distance $r=|\vec{r}_1-\vec{r}_2|$. This is equivalent to the assumption that the intermediate nucleon momentum q of Fig. 3 is small compared to its mass M. This is a reasonable approximation because $q<p\sim\sqrt{mM}\ll M$, where p is the momentum of each outgoing nucleon.

In order to evaluate the importance of the diagrams of Fig. 3 as compared to those of Fig. 2, we chose the case of π^- absorption on a deuteronlike pair of nucleons. For the initial state we assume the presence of an s-state wave function for this initial deuteron, and, similarly for the final state, we suppose plane waves for the outgoing nucleons multiplied by a spherically symmetric function (such as a correlation function). The particular choice is irrelevant for purposes of comparison with the diagram of Fig. 2, since in the following expressions we keep only the plane wave function that is necessary for the angular integrations and omit all the other radial functions. We also suppress the overall momentum conservation δ function.

The matrix element for the s-wave rescattering, Eq. (3), is then

$$S_1=\sqrt{2}\ 130\pi^2 g^3 i(\vec{\sigma}_1+\vec{\sigma}_2)\cdot\hat{p}mj_1(pr)\times\int_0^\infty \frac{k^3dk\,j_1(kr)}{(k^2+\frac{3}{4}m^2)}\left[\frac{j_1(kR)}{kR}\right]^2. \tag{6}$$

In Eq. (6) we have chosen the final nucleons to have equal energies,

$$E_{1,2}=M+\frac{m}{2}\ ;$$

this is appropriate to the kinematical situation in which all three initial particles are at rest.

Using Eqs. (2)—(5) we obtain the matrix element for the diagrams of Fig. 3. Summing the contributions from the first two and the last two diagrams, amongst which there is some cancellation, we find (neglecting small terms)

$$S_2=-\frac{\sqrt{2}i\,108g^5}{(2\pi)^3}\int\frac{d\Omega_{\hat{r}}d^3k\,d^3k'e^{i(\vec{k}-\vec{k}')\cdot\vec{r}}e^{-i\vec{p}\cdot\vec{r}}}{(k^2+m^2)(k'^2+\frac{3}{4}m^2)((\vec{k}-\vec{k}')^2+\frac{3}{4}m^2)}\times[O_1(\vec{k},\vec{k}')\vec{\sigma}_1\cdot(\vec{k}-\vec{k}')-O_2(\vec{k},\vec{k}')\vec{\sigma}_2\cdot(\vec{k}-\vec{k}')]\vec{k}\cdot\vec{k}'\frac{j_1(k'R)}{kR}\frac{j_l(k'R)}{k'R}\frac{j_1(|\vec{k}-\vec{k}'|R)}{|\vec{k}-\vec{k}'|R}, \tag{7}$$

where

$$O_1(\vec{k},\vec{k}')=\tfrac{17}{8}m^2+\tfrac{3}{2}k^2-\tfrac{1}{2}k'^2+2\vec{k}\cdot\vec{k}' \tag{8}$$

and

$$O_2(\vec{k},\vec{k}')=\tfrac{3}{4}m^2+k'^2-k^2\ . \tag{9}$$

[We also checked Eqs. (6) and (7) by direct calculation using standard prescriptions for relativistic Feynman di-

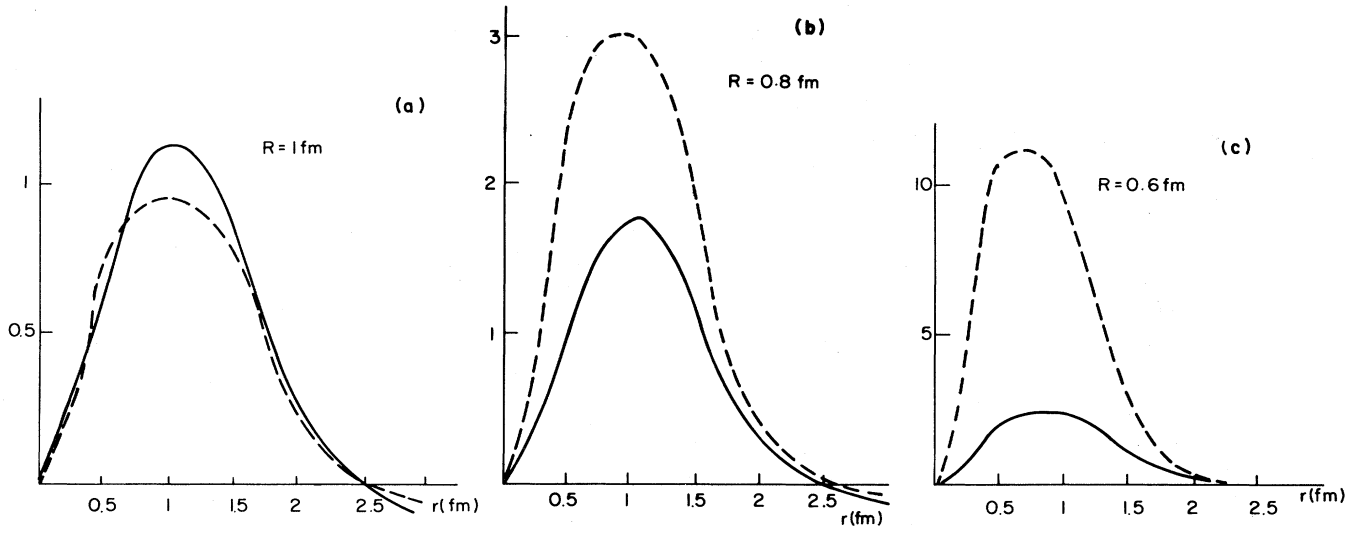

FIG. 5. Single-pion rescattering (full line) and third-order pion contribution (dashed line) for $R=1$ fm [(a)], 0.8 fm [(b)], and 0.6 fm [(c)]. The ordinate is to be multiplied by $24\sqrt{2}$ to obtain the quantities of Eqs. (6) and (11).

agrams, taken to the nonrelativistic limit.] We next exploit the relation

$$\frac{3j_1(|\vec{k}-\vec{k}'|R)}{|\vec{k}-\vec{k}'|R}=\frac{\omega_0}{8\pi(\omega_0-1)j_0^2(\omega_0)R^3}\int_0^R d^3x\, e^{i(\vec{k}-\vec{k}')\cdot\vec{x}}(j_0^2(\omega_0 x/R)+j_1^2(\omega_0 x/R))$$

$$=\frac{\omega_0}{2(\omega_0-1)j_0^2(\omega_0)R^3}\int_0^R x^2dx\sum_{l=0}^{\infty}P_l(\hat{k}\cdot\hat{k}')(2l+1)j_l(kx)j_l(k'x)$$

$$\times(j_0^2(\omega_0 x/R)+j_1^2(\omega_0 x/R))\,, \tag{10}$$

where $\omega_0=2.04$ is the lowest bag eigenmode, and develop the denominator $(\vec{k}-\vec{k}')^2+\frac{3}{4}m^2$ in Legendre polynomials $P_l(\hat{k}\cdot\hat{k}')$, obtaining a double series whose convergence was checked numerically. The maximum error in the overall third-order amplitude caused by this procedure was $\sim 2\%$. To this accuracy the expression of Eq. (7) becomes

$$S_2\cong -288g^5 i\sqrt{2}\int\frac{k^2dk\,k'^2dk'x^2dx\,j_1(pr)j_1(kR)j_1(k'R)}{(k^2+m^2)(k'^2+\frac{3}{4}m^2)}\{f_2(k,k')\vec{\sigma}_1\cdot\hat{p}-f_1(k,k')\vec{\sigma}_2\cdot\hat{p}\}\,, \tag{11}$$

where f_1 and f_2 are given in the Appendix.

Performing the integrations of Eqs. (6) and (11) numerically, we evaluate the importance of the diagrams of Fig. 3 relative to those of Fig. 2. We find that the contributions due to f_2 are greater by roughly an order of magnitude than those of f_1, and so we have dropped the f_1 term. Note that for the specific spin states the contributions of f_1 may not be negligible; we present here results for the coefficient of $i(\vec{\sigma}_1+\vec{\sigma}_2)\cdot\hat{\vec{p}}$ in S_1 and $i\vec{\sigma}_1\cdot\hat{\vec{p}}$ in S_2. Figures 5(a)—(c) display these results for bag radii of $R=1$, 0.8, and 0.6 fm, which are in the range of acceptable values. It is readily seen that the diagrams of Fig. 3 are as important as those of Fig. 2 for internucleon distances $r\lesssim 2$ fm, but of course, are less important for $r>2$ fm; they may dominate for $r\lesssim 1$

fm for a bag radius of $R=0.6$ fm. These characteristics arise because the diagrams of Fig. 3 involve more massive exchange than the single pion in Fig. 2. Note that the two-pion exchange of Fig. 3 carries the opposite sign compared to the amplitude of Fig. 2, and therefore tends to cancel the one-pion exchange. This is similar to the usual effect of ρ exchange, itself a (resonating) two-pion exchange effect.[11] If instead of a bag model form factor one chooses to use the customary monopole vertex function $\Lambda^2/(\Lambda^2+k^2)$, k being the momentum transfer and Λ a cutoff parameter, we find analogous results provided that there is a straightforward identification between R and Λ. The one pion exchange potential calculation suggests that $R=1$, 0.8, and 0.6 fm correspond well with $\Lambda=3$, 4, and 5.5 fm^{-1}, and we have verified that similar results are then obtained for our process here.

We have also calculated the soft pion limit $m\to 0$ of Eq. (11) and obtained the results displayed in Fig. 6. The curve shows almost constant behavior for 50 MeV $< m \leq 140$ MeV, and then an abrupt fall towards zero. A similar trend was found by Afnan and Thomas[12] for the sum of the terms of first and second order, Figs. 1 and 2, using an explicit deuteron wave function in $\pi^+ d\to pp$.

Finally, we conclude that the third-order rescattering diagrams calculated in the framework of a chiral bag model Lagrangian make a very appreciable contribution to pion absorption on two nucleons and thus must be included on the same level as other higher-order effects such as the s-wave rescattering with single pion exchange. In a complete calculation, one must also consider graphs in which the inner baryon lines become isobaric resonances, rather than nucleons, as well as diagrams where heavy mesons are exchanged. This latter extension would be better performed without the inclusion of ρ exchange, which risks being redundant with isovector parts of the two-pion transfer included here. Unfortunately, there does not seem to exist at present a well founded theoretical basis on which to distinguish between such effects, so that their further study would have to be carried out phenomenologically.

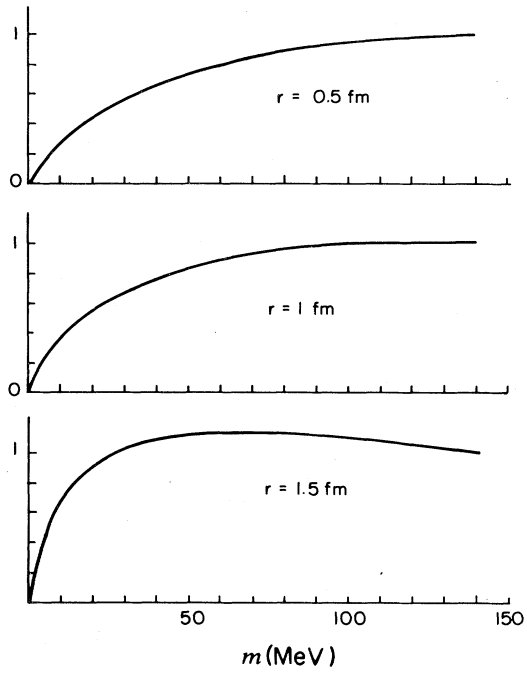

FIG. 6. Soft pion ($m\to 0$) limit for the diagrams of Fig. 3 for three internucleon distances, from top to bottom: $r=0.5$, 1, and 1.5 fm; $R=0.6$ fm. The curves are normalized to one at $m=140$ MeV.

This work was supported in part by the U.S.-Israel Binational Science Foundation and by the Israel Academy of Science and Humanities, Basic Research Foundation.

APPENDIX

The functions f_1, f_2 are given by

$$f_l=\frac{1}{z}\left[\left[\sum_{i=1}^{4}a_i\left[\frac{2}{z}\right]^{i-1}\right](u_0-2.5u_2)Q_l+\left[\sum_{i=2}^{4}a_i\left[\frac{2}{z}\right]^{i-2}\right]\left[lu_0+\frac{3Q_l}{kk'}(u_1-3.5u_3)\right]\right.$$
$$\left.+\left[a_3+\frac{2a_4}{z}\right]\left[\frac{3l}{kk'}(u_1-3.5u_3)+7.5\frac{u_2Q_l}{(kk')^2}\right]+a_4\left[\frac{7.5lu_2}{(kk')^2}+\frac{17.5Q_lu_3}{(kk')^3}\right]\right], \tag{A1}$$

where

$$z=k^2+k'^2+\tfrac{3}{4}m^2\ , \tag{A2}$$

$$u_n(x)=\frac{\omega_0}{2(\omega_0-1)j_0^{\,2}(\omega_0)R^3}(j_0^{\,2}(\omega_0 x/R)+j_1^{\,2}(\omega_0 x/R))j_n(kx)j_n(k'x)\ , \tag{A3}$$

$$Q_2=\tfrac{17}{8}m^2+\tfrac{3}{2}k^2-\tfrac{1}{2}k'^2\ , \tag{A4}$$

$$Q_1=\tfrac{3}{4}m^2+k^2+k'^2\ , \tag{A5}$$

and

$$a_1=\left[b_1\left[kc_2-\frac{c_1}{x}\right]+c_1\left[k'b_2-\frac{b_1}{x}\right]\right]kk'\ ,$$

$$a_2=\left[b_2\left[kc_3-\frac{c_2}{x}\right]+\frac{kb_1c_1}{k'x}+c_2\left[k'b_3-\frac{b_2}{x}\right]+\frac{k'b_1c_1}{kx}\right](kk')^2\ ,$$

$$a_3=[2kb_3c_4-12b_3c_3/x+3b_1(kc_2-c_1/x)+2k'c_3b_4+3c_1(k'b_2-b_1/x)]\frac{(kk')^3}{5}\ ,$$

$$a_4=\left\{8kb_4c_5-64b_4c_4/x+8k'c_4b_5+30\left[b_2(kc_3-6c_2/x)+\frac{kb_1c_1}{k'x}+c_2k'b_3+\frac{k'b_1c_1}{kx}\right]\right.$$
$$\left.-3(kb_0c_1+k'c_0b_1)\right\}\frac{(kk')^4}{35}\ ,$$

with

$$b_l=j_l(k'x),\quad c_l=j_l(kx)\ .$$

[1]D. S. Koltun and A. Reitan, Phys. Rev. 141, 1413 (1966).

[2]K. Shimizu and A. Faessler, Phys. Rev. C 17, 1891 (1978).

[3]S. Weinberg, Phys. Rev. Lett. 18, 188 (1967).

[4]G. E. Brown, M. Rho, and V. Vento, Phys. Lett. 84B, 383 (1979).

[5]S. Théberge, A. W. Thomas, and G. A. Miller, Phys. Rev. D 22, 2838 (1980); 23, 2106(E) (1981); A. W. Thomas, J. Phys. G 7, L283 (1981).

[6]C. Detar, Phys. Rev. D 24, 752 (1981); 24, 762 (1981).

[7]G. Kälbermann and J. M. Eisenberg, Phys. Rev. D (to be published).

[8]G. Kälbermann and J. M. Eisenberg, Phys. Rev. D (to be published).

[9]A. Chodos, R. L. Jaffe, K. Johnson, and V. F. Weisskopf, Phys. Rev. D 9, 3471 (1974).

[10]T. DeGrand, R. L. Jaffe, K. Johnson, and J. Kiskis, Phys. Rev. D 12, 2060 (1979).

[11]M. Brack, D. O. Riska, and W. Weise, Nucl. Phys. A287, 425 (1977).

[12]W. R. Afnan and A. W. Thomas, Phys. Rev. C 15, 2143 (1977).